LA-UR- 97-4830

Evidence of plasma fluctuations and their effect on the growth of stimulated Brillouin and stimulated Raman scattering in laser plasmas*

CONF-971103--

D.S. Montgomery†, J.C. Fernández, J.A. Cobble, M.D. Wilke, E.L. Lindman, H.A. Rose, B.H. Wilde, D.F. Dubois, B. Bezzerides, and H.X. Vu

Los Alamos National Laboratory, Los Alamos, New Mexico 87545

B.J. MacGowan, S.H. Glenzer, R.K. Kirkwood, J.D. Moody, and D.H. Munro

Lawrence Livermore National Laboratory, Livermore, California 94551

B.B. Afeyan

University of California, Davis-Livermore, Livermore, California 94551

The reflectivity levels of stimulated Brillouin scattering (SBS) in recent large scale length laser plasma experiments is much lower than expected for conditions where the convective gain exponent is expected to be large [J.C. Fernández *et al.*, Phys. Plasmas **4**, 1849 (1997)]. Long wavelength velocity fluctuations caused during the plasma formation process, or by parametric instabilities themselves, have been proposed as a mechanism to detune SBS in these experiments and reduce its gain [W.L. Kruer *et al.*, Phys. Plasmas **3**, 382 (1996), H.A. Rose, Phys. Plasmas **4**, 437 (1997)]. Evidence of large velocity fluctuation levels is found in the time-resolved SBS spectra from these experiments, and correlates with observed changes in the reflectivity of both SBS and stimulated Raman scattering (SRS). We present evidence of fluctuations which increase as the plasma density systematically increases, and discuss their effect on the growth of parametric instabilities.

PACS: 52.35.Nx, 52.40.Nk, 52.50.Jm

†Invited speaker

*Paper mWepI1.03, Bull. Am. Phys. Soc. (1997)

DISCLAIMER

I. Introduction

Understanding the growth and saturation of laser-driven parametric instabilities such as stimulated Brillouin scattering (SBS) and stimulated Raman scattering (SRS) is important for the success of laser fusion. These instabilities can occur throughout the underdense plasma in targets designed to achieve ignition, such as those for the proposed National Ignition Facility (NIF), and are a concern since they can scatter a significant fraction of laser energy. Predicting the onset and saturated reflectivity of these instabilities under given laser and plasma conditions is the goal of research in this field, and will lead ultimately to their control.

Both SBS and SRS are three-wave processes involving the resonant decay of the incident laser wave into a scattered light wave and a plasma wave. The instabilities must satisfy the frequency and wave-vector matching conditions

$$\begin{aligned} \omega_0 &= \omega_s + \omega_{es} \\ \vec{k}_0 &= \vec{k}_s + \vec{k}_{es} \end{aligned} \tag{1}$$

where ω, $\vec{k}$ are the frequency and the vector wavenumber, and the subscripts 0, s, es refer to the incident, scattered, and electrostatic plasma waves. For SBS, the plasma wave is a low-frequency ion acoustic wave, whose dispersion is approximately $\omega_{es} \cong c_s k_{es} + \vec{v} \cdot \vec{k}_{es}$, where c_s is the sound speed and v is the local flow velocity. The plasma wave involved in the SRS process is an electron-plasma wave, with a frequency given approximately by the Bohm-Gross dispersion $\omega_{es}^2 \cong \omega_p^2 + 3k_{es}^2 v_{th}^2$, where ω_p is the well-known electron plasma frequency, and v_{th} is the electron thermal speed. Hereafter, the frequency and wavenumber for ion-acoustic waves (IAW) will be denoted by ω_{ia}, k_{ia}, and for electron-plasma waves (EPW) by ω_{epw}, k_{epw}.

The resonance conditions imply that frequency and wavenumber matching for a given unstable mode are satisfied only in a narrow range of plasma parameters, i.e. SRS is

sensitive mostly to density inhomogeneitiy, and SBS is sensitive mostly to sound speed and velocity inhomogeneities. The theory for the linear growth of SRS and SBS in idealized plasma conditions is well known [1], and the amplification factors predicted for current experiments are usually very large ($\geq$ exp [20]) such that nonlinearities are expected to limit instability growth.

Recent experiments have been performed in large scale length plasmas [2-8] that mimic conditions in certain regions of NIF ignition targets which are expected to have large instability growth factors. One suprising result from these experiments is that the SBS reflectivity is quite low (~ 1 %) for certain laser and plasma conditions whieh are expected to produce much larger amplification [2]. Several possible mechanisms have been proposed to explain the low SBS reflectivities observed in experiments, including ion-tail heating [9] and secondary decay mechanisms [10, 11]. More recently, it has been proposed that non-ideal plasma conditions exist in the form of long-wavelength density and velocity fluctuations which could limit the SBS amplication to low values [12-14]. These fluctuations may be driven by the plasma heating process [12, 13], by profile modification due to momentum deposition [15], or by the effects of non-local heat transport within laser hot spots [16].

In this paper we report experiments which measure the saturated levels of SRS and SBS over a broad range of plasma densities and IAW damping. The plasma density and IAW damping are systematically controlled using preheated gas-filled targets, which produce quasi-homogeneous, large scale length, hot plasmas (L ~ 2mm, T_e ~ 3 keV). The long-time behavior of the SRS and SBS reflectivity is found to depend on the hydrodynamic evolution of the plasma conditions. The observed experimental trends are that SRS increases as density increases, as expected from simple linear theory since the EPW damping decreases significantly. However, SBS is observed to decrease with increasing density, contrary to simple theory, and decreases dramatically (orders of magnitude) in the strongly damped regime, and decreases only moderately in the weakly

damped regime. Moreover, the SBS spectra broaden with increasing density, and are found to correlate with changes in SBS reflectivity. In Sec. II, the laser and plasma conditions for these experiments are described. In Sec. III, we discuss the effect of the "blast-wave" on the growth of SRS and SBS in these gas-filled target experiments. Section IV describes the evidence of velocity fluctuations and their correlation with SBS reflectivity, and Sec. V presents a model describing the effect of long-wavelength velocity fluctuations on SBS growth. The summary and conclusions are given in Sec. VI.

II. Laser and Plasma Conditions

The experiments were carried out using nine beams of the NOVA laser [17] to preheat a gas-filled target, which was either a LLNL-designed gasbag [7], or a LANL-designed toroidal hohlraum [3]. The targets have thin "windows" made of either 0.3-μm thick polyimide (LLNL gasbag), or of 0.25-μm thick silicon nitride (LANL hohlraum), and are inflated to ~ 1 atm pressure with various gas mixtures. The nine heater beams are unsmoothed, and have ~ 10:1 intensity modulations over ~ 100 μm spatial scales, typical of high-power glass lasers. A tenth "interaction" beam is used to drive SRS and SBS after the plasma has been heated, and the reflected energy and time-resolved spectra are measured in the backscatter direction using calorimetry and streaked spectroscopy [7]. The 351 nm interaction beam is focused using an f/4 lens, and is spatially smoothed using a random phase plate [18]. The average interaction beam laser intensity is typically ~ 2 x 10^{15} W/cm^2 for these experiments, and has a flat-topped 1 ns pulse duration. For the LLNL gasbag experiments, the nine heater beams are flat-top 1 ns pulses, and the interaction beam is delayed 0.5 ns after the start of the heaters, such that there is ~0.5 ns overlap between the heaters and the interaction beam. For the LANL gas-hohlraum experiments, the heater beams have a 1.5 ns trapezoidal pulse shape, and the interaction beam is also delayed 0.5 ns after the start of the heaters. Additional LLNL gasbag experiments have been performed

using 1.5 ns heater beams, and show little difference in SRS and SBS reflectivities compared to experiments with 1 ns heater beams.

The fill-gas for these experiments is selected in order to systematically vary the plasma density and IAW damping. For plasmas with weak IAW damping, a mixture of CO_2 and CF_4 gases is used to produce an average density in the range of $n_e/n_{cr} = 0.06$ - 0.15, where ncr is the critical density for 351 nm light. To achieve plasmas with strong IAW damping, gas mixtures containing hydrogen such as C_3H_8, C_4H_{10}, and C_5H_{12} are used to vary the average density over this same range. Plasmas with intermediate IAW damping are produced using gas mixtures with varying fractions of C_nH_{2n+2} gas combined with CO_2/CF_4 mixtures. By the time that the interaction beam turns on at 0.5 ns, the plasma is heated typically to ~ 3 keV, and has a density and velocity gradient scale length ~ 2 mm (neglecting fluctuations which will be discussed later). A schematic of the LLNL gasbag and LANL gas-hohlraum targets is shown in Fig. 1. The targets were designed to produce bulk plasma conditions which are similar for a given gas mixture, although there are some detailed differences.

Simulations using the radiation hydrodynamics code LASNEX [19] have been performed for various gas-fills in these two target geometries, and profiles of typical plasma conditions along a laser ray path are also shown in Fig. 1. The calculations at 0.7 ns show a T_e ~ 3 keV isothermal plasma, with a ~ 1 mm length density plateau at the average density expected for the completely ionized gas. A "blast-wave", due to the explosion of the skin pushing on the gas, propagates inward at ~ 5 x 10^7 cm/s, with a corresponding rarefaction wave traveling outward. The effects of the "blast-wave" on the long-time temporal evolution of SRS and SBS is discussed next.

III. Effect of "blast-wave" on evolution of SRS and SBS

Although LASNEX calculations show some detailed differences in the plasma profiles between gasbag and gas-hohlraum targets, the SRS and SBS spectra from these

two targets show quite similar features. Figure 2 shows the time-resolved backscattered SRS and SBS spectra from LLNL gasbag and LANL hohlraum experiments with n_e/n_{cr} ~ 0.11 and $\nu_{ia}/\omega_{ia} > 0.1$, where ν_{ia}/ω_{ia} is the normalized IAW damping rate. The interaction beam turns on at 0.5 ns for both experiments, and the SRS starts immediately. The SRS scattered spectra are fairly narrow at this time (~ 15 nm), and correspond to "normal" scattering from the expected average plasma conditions n_e/n_{cr} ~ 0.11 and T_e ~ 3 keV. Later in time (~ 1 ns), a temporary disruption in the "normal" SRS occurs, and is coincident with a longer-wavelength feature (600 - 650 nm) corresponding to higher densities. The "normal" SRS then recovers after ~ 250 ps, and continues until the end of the interaction pulse. The higher density SRS is attributed to the "blast-wave", and will be discussed later in this section.

The SBS spectra were measured simultaneously on these experiments, and are also shown in Fig. 2. Before 0.5 ns, sidescattering from the heater beams is observed. SBS produced from the interaction beam starts weakly at 0.5 ns, and is observed to peak at ~ 1 ns coincident with the disruption in "normal" SRS and with the observation of "blast-wave" SRS. The SBS suddenly decreases before the end of the interaction pulse. The centroid of the SBS spectral shift is ~ 10 Å, which is expected from a "stationary" 3 keV plasma. Further details of the time-resolved SBS reflectivity and spectra will be discussed later in Sec. IV.

A coincidence is observed in timing between the disruption of "normal" SRS, the onset of "blast-wave" SRS, and the peak of SBS over a range of n_e/n_{cr} and ν_{ia}/ω_{ia}. It is found that for lower n_e/n_{cr} these features all occur earlier in time (~ 0.8 ns) compared to higher n_e/n_{cr}. Since these detailed features are quite similar for both LANL gas-hohlraums and LLNL gasbags, the similar plasma conditions of a large, quasi-homogeneous density plateau with an inward propagating high-density "blast-wave" is a probable cause for these spectral features. To test this, experiments with "stretched" LANL gas-hohlraums were

performed, where the target length was increased 0.25 mm compared to "unstretched" hohlraums. LASNEX calculations showed that the "blast-wave" arrives at a given point ~ 200 ps later in the "stretched" target compared to the "unstretched" target. Figure 3 shows SRS and SBS time-resolved spectra from an "unstretched" and a "stretched" hohlraum filled with C_3H_8 to give an average density of $n_e/n_{cr} \sim 0.06$. The two targets are expected to produce otherwise similar plasma conditions. The experiments show that the "normal" SRS disruption, onset of "blast-wave" SRS, and peak SBS all occur at 0.8 ns for the "unstretched" hohlraum, and are also coincident but delayed to 1.0 ns for the "stretched" hohlraum. This delay is consistent with LASNEX predictions, which suggests that these changes in the SRS and SBS growth late in time are affected by the "blast-wave".

To better understand what role the "blast-wave" plays in determining the growth of SRS and SBS, instability gain calculations were performed using profiles of the plasma conditions from LASNEX simulations. The convective gain exponent as a function of scattered light wavelength was calculated in the strong damping limit using a standard formula [20], and the kinetic dispersion relations. The spatial gain rate $\kappa(z, \lambda)$ for either SRS or SBS was calculated at different times using the LASNEX profiles. Integration of $\kappa(z, \lambda)$ over a region gives the convective gain $G(\lambda)$ for that region. Figure 4a shows a calculationof $\kappa(z, \lambda)$ for SRS using a LASNEX simulation profile for a C_5H_{12} 0.11 n_{cr} plasma at the start of the interaction beam at 0.5 ns. The spatial gain was calculated from profiles at various time steps, and integrated to produce time-dependent spectra of $G(\lambda)$, which are shown in Figs. 4b and 4c. The SRS gain spectra in Fig. 4b is produced by integrating $\kappa(z, \lambda)$ over the entire region, and shows the SRS gain gradually decreasing in time as the plasma scalelength decreases due to the inward moving blast-wave. The SRS gain is peaked mostly at a wavelength corresponding to the average plasma density, although some SRS gain is evident at longer wavelengths due to the blast-wave. Figure 4c

is produced by integrating only over a limited region from z=0.6 to 1.2 mm, and shows that as the blast-wave propagates into this region, the "normal" SRS from the average density is disrupted and is coincident with seeing SRS gain from the blast wave. As the blast-wave propagates further, the "normal" SRS gain recovers. This behavior should be qualitatively compared with the experimental SRS spectra shown in Fig. 2a, and suggests that SRS may be growing only in a limited region rather than throughout the entire laser-plasma volume. A similar effect is also observed for gain calculations of LANL gas-hohlraums. Gain calculations of SBS for these two targets also suggest that SBS is coming from a limited interaction region, and the gain rapidly decreases once the blast wave has propagated into this region, resulting in higher ion temperatures and stronger damping.

IV. Evidence of fluctuations and correlation with SBS

Several experiments were performed using LLNL gasbags that systematically varied the average density from $n_e/n_{cr} = 0.06 - 0.15$, in either the strong IAW damping limit ($\nu_{ia}/\omega_{ia} \sim 0.3$), or in the weak IAW damping limit ($\nu_{ia}/\omega_{ia} \sim 0.01$). As shown previously in Fig. 2b, the SBS reflectivity is peaked at 0.8 - 1.0 ns, and does not last the entire interaction pulse duration. Figure 5 shows a plot of peak SBS reflectivity and the SRS reflectivity at that same time versus n_e/n_{cr}. The data are shown for both strong IAW damping (C_3H_8/C_5H_{12} gases) and weak IAW damping (CO_2/CF_4 gases). The SRS increases with increasing density, as expected from simple linear theory since the EPW damping rate decreases dramatically over this range of density. The SRS levels are ~ 10-20x lower over the range of n_e/n_{cr} compared to strong IAW damping, consistent with previous experiments [3, 4] which show the dependence of saturated SRS on IAW damping. The SRS saturation mechanism proposed in Refs. 3 and 4 is due to a secondary coupling of the SRS EPW with an IAW, either from the Langmuir decay instability (LDI) or the electromagnetic decay instability (EDI).

A striking trend in these experiments is that the SBS levels for strong IAW damping decrease dramatically as n_e/n_{cr} increases, in contrast to simple theory, and are anti-correlated with SRS levels. Anti-correlation is also observed between SBS and SRS in the weak IAW damping regime, although the decrease of SBS with n_e/n_{cr} is only moderate. Some experiments have been performed using LANL gas-hohlraums, and similar trends are observed as gasbags, although the database is much less extensive.

The SBS spectral shift for these experiments is consistent with SBS from a ~ 3 keV, quasi-stationary plasma, and is ~ 9 Å at the time of peak reflectivity. SBS from the blast-wave region would produce a shift either more red or blue, depending on which side of the blast-wave it is occuring. Detailed analysis shows that the SBS spectra broaden as n_e/n_{cr} increases, and is shown in Fig. 6 for gasbag experiments with weak IAW damping. A similar broadening is observed for strong IAW damping experiments. To quantify the spectral broadening, a normalized width $\Delta\omega/\omega_{ia}$ was determined by measuring the spectral FWHM, corrected for instrument resolution, and dividing by the spectral shift. Plots of the time-dependent SBS reflectivity and normalized width $\Delta\omega/\omega_{ia}$ are shown in Figs. 7 for a low density CO_2 gasbag experiment, and a low density CF_4/C_4H_{10} (ν_{ia}/ω_{ia} ~ 0.05) gas-hohlraum experiment. The time-dependent spectra show that the peak SBS reflectivity occurs when $\Delta\omega / \omega_{ia}$ is smallest, and low SBS corresponds to large $\Delta\omega / \omega_{ia}$.

The data show a clear trend of increasing spectral width $\Delta\omega/\omega_{ia}$ as SBS reflectivity decreases. Assuming no ambient flow gradients occur, the normalized spectral width $\Delta\omega/\omega_{ia}$ indicates the level of velocity fluctuations occuring within the SBS interaction region. It is well known that such fluctuations can detune the gain for SBS [12-14], and the trend indicates that SBS reflectivity decreases as the velocity fluctuation level increases. Next, we discuss how such fluctuations might arise in these experiments, and describe a model for their effect on SBS.

V. Theory and Modeling

Large levels of long-wavelength velocity fluctuations might arise and increase with n_e/n_{cr} in these experiments through several different processes. The nine beams used to create the plasma are unsmoothed, and have significant intensity modulations over spatial scales of ~ 100 μm. As the unsmoothed beams heat the windows and cold gas, both density and velocity pertubations can arise due to filamentation, and are expected to increase with n_e/n_{cr}. This effect may be more pronounced in gasbags since the entire plasma volume is directly heated with unsmoothed beams, whereas the interaction volume in gas-hohlraums is heated by conduction from the surrounding heater beam regions. Effects of the unsmoothed heater beams is not included in the LASNEX calculations.

Additionally, the speed of the ionization front early in the gas heating is finite [21], and the huge pressure gradient between the heated plasma and cold gas imparts an impulse to the plasma, creating fluctuations early in time. This effect is seen in LASNEX calculations, as evidenced in the SRS spatial growth rate plot shown in Fig. 4a, and increases with n_e/n_{cr} since the ionization front speed decreases with density [21].

Finally, fluctuations may be created by the interaction beam, either from the instabilities themselves, or due to transport effects. A recent theory [15] suggests that the flow-profile within a hot spot can be modified due to momentum deposition of the scattered waves, thus detuning SBS within each hot spot. According to estimates given in Ref. 15 for conditions similar to these experiments, a velocity Mach number fluctuation M ~ 0.3 is easily attained within a hot spot with modest SRS reflectivity. Another recent paper [16] suggests that flat-top electron distributions inside hot spots, due to transport effects, will cause the EPW damping to decrease substantially and the sound speed to increase up to 20% within a given hot spot, and depends on the local hot spot intensity. Changes in c_s within localized regions introduces an effective fluctuation level, so that detuning of SBS will occur from this effect alone. The additional effect of decreasing EPW damping means

that SRS can occur more easily within a hot spot, possibly creating turbulence and detuning SBS.

To assess the effects of fluctuations on SBS growth, a WKB formula [13] is used to calculate SBS gain in fluctuating plasmas for all ion wave damping rates

$$\kappa(z) = -\frac{1}{2}(\nu_{IAW} + iD) + \sqrt{\left[\frac{1}{4}(\nu_{IAW} + iD)^2 + \frac{\Gamma_0^2}{V_1 V_2}\right]} \qquad (2)$$

$$D(z) = \Delta\omega - \sum_{i=1}^{N} M_i(0)\left[\sin\left(k_u^{(i)} z - \phi_i\right) - \sin(\phi_i)\right] \qquad (3)$$

where $\kappa(z)$ is the spatial gain rate for SBS, and $D(z)$ is the detuning function, represented here by sine waves with random amplitudes M_i, wavenumbers k_u and phases φ_i. The temporal growth rate Γ_0, the IAW damping rate ν_{IAW}, the group velocities $V_1 V_2$, and the frequency detuning $\Delta\omega$ are all given in normalized (dimensionless) units. An average fluctuation level M_{RMS} can be determined from the root-mean-square value of the detuning function D(z). Figure 8a shows a typical plot of D(z) for $\Delta\omega$=0, obtained by adding 5 modes with wavelengths between 100 and 200 μm, and $M_{RMS} = 0.3$.

Several calculations were carried out, varying only M_{RMS} and ν_{IAW}, and the growth rate and group velocities were selected using typical laser and plasma conditions in these experiments. The calculated SBS gain is shown in Fig. 8b for various IAW damping rates versus fluctuation level M_{RMS}. For $\nu_{ia}/\omega_{ia} = 0.3$, the SBS gain is reduced from G=22 to a small convective gain G=13 for a fluctuation level $M_{RMS} = 0.3$. In the case of strongly damped SBS, the fluctuations cause a tremendous decrease in convective amplification. The weakly damped regime ($\nu_{ia}/\omega_{ia} = 0.01$) shows that SBS decreases from an absolute instability to a high gain convective instability (G ~ 30) when $M_{RMS} = 0.3$. These calculations demonstrate that SBS convective amplification is dramatically affected by

fluctuations in the strongly damped regime, but moderately affected in the weakly damped regime. This is qualitatively consistent with the observed experimental trends.

The SBS gain spectra are also calculated, and the normalized spectral width $\Delta\omega/\omega_{ia}$ is plotted in Fig. 8c for various IAW damping rates and M_{RMS} levels. The spectral width increases with M_{RMS} for all IAW damping rates, and $\Delta\omega/\omega_{ia} \sim M_{RMS}$ appears to be a reasonable lower bound. The spectral width is larger in the strong damping regime The calculation of $\Delta\omega/\omega_{ia}$ accounts for gain narrowing, but neglects any nonlinearity in the growth of SBS.

VI. Discussion and Conclusions

The observed experimental trends in SBS are consistent with a model of long-wavelength fluctuations which increase with density, and explains the decrease of SBS in the weak and strong IAW damping regimes, and the SBS spectral broadening. In the strong damping regime, a fluctuation level $M_{RMS} \sim \nu_{ia}/\omega_{ia} \sim 0.3$ is sufficient to cause a dramatic decrease in SBS reflectivity, as observed in the experiments. It is reasonable to assume that SBS is convective in the strongly damped regime, and would require a gain length greater than several hot spot lengths in order to achieve appreciable gain. A fluctuation level $M_{RMS} \sim 0.3$ is not unreasonable, based on the measured SBS spectral widths, and assuming that the fluctuation processes discussed in Sec. V yield reasonable estimates. In the weak damping regime, the SBS gain length is much less than a hot spot length, so that high convective gain is still realized in the presence of large fluctuations.

Although not discussed in Sec. V, velocity fluctuations can also have an effect on SRS reflectivity, since the SRS saturation mechanism (LDI or EDI) involves coupling into an IAW. The growth of the IAW from LDI or EDI would also be detuned by velocity fluctuations, thus allowing SRS growth to a higher saturated level. The calculated effects of

velocity fluctuations on LDI and EDI growth is beyond the scope of this Paper, but is expected to behave qualitatively similar to SBS since the IAWs for SBS and LDI/EDI have similar wavelengths. Anti-correlation is expected between SRS and SBS with this fluctuation model, since SBS and LDI/EDI growth are detuned, resulting in lower SBS and higher SRS.

In summary, experiments with gas-filled targets show several interesting trends. The "blast-wave" caused during the plasma formation process affects the long-time behavior of SRS and SBS, and may explain why features in the SRS and SBS spectra are correlated in time. There is an anti-correlation between SRS and SBS levels over a wide range of plasma density and IAW damping. The SBS reflectivity is dramatically reduced at high density in the strong IAW damping regime, and moderately reduced in the weak damping regime. The SBS spectral width is observed to increase with increasing density, and correlates with a reduced SBS reflectivity, even for time-dependent measurements. Finally, a model is proposed which shows that long-wavelength velocity fluctuations are a likely explanation for the observed SBS trends.

Acknowledgements

We thank the LLNL Nova operations staff and the LANL technicians for their dedicated support in these experiments, Pete Gobby (LANL), Gary Stone (LLNL), and the LANL and LLNL target fabrication teams, and W.L. Kruer, B.F. Lasinski, R.L. Berger, E.A. Williams at LLNL for useful discussions. This work was performed under the auspices of the U.S. Department of Energy by Los Alamos National Laboratory under contract number W-7405-Eng-36.

References

1. M.N. Rosenbluth, Phys. Rev. Lett. **29**, 565 (1972)

2. L.V. Powers, R.L. Berger, R.L. Kauffman, B.J. MacGowan, P.A. Amendt, C.A. Back, T.P. Bernat, S.N. Dixit, D.I. Eimerl, K.G. Estabrook, J.A. Harte, D.H. Kalantar, D.E. Klem, B.F. Lasinski, D.S. Montgomery, J.D. Moody, D.H. Munro, T.D. Shepard, L.J. Suter, R.E. Turner, E.A. Williams, J.C. Fernández, W.W. Hsing, B.H. Wilde, B.H. Failor, Phys. Plasmas **2**, 2473(1995).

3. J.C. Fernández, J.A. Cobble, B.H. Failor, D.F. Dubois, D.S. Montgomery, H.A. Rose, H.X. Vu, B.H. Wilde, M.D. Wilke, and R.E. Chrien, Phys. Rev. Lett. **77**, 2702 (1996).

4. R.K. Kirkwood, B.J. MacGowan, D.S. Montgomery, B.B. Afeyan, W.L. Kruer, J.D. Moody, K.G. Estabrook, C.A. Back, S.H. Glenzer, M.A. Blain, E.A. Williams, R.L. Berger, and B.F. Lasinski, Phys. Rev. Lett. **77**, 2706 (1996).

5. J.C. Fernández, B.S. Bauer, J.A. Cobble, D.F. Dubois, G.A. Kyrala, D.S. Montgomery, H.A. Rose, H.X. Vu, R.G. Watt, B.H. Wilde, M.D. Wilke, W.M. Wood, B.H. Failor, R. Kirkwood, and B.J. MacGowan, Phys. Plasmas **4**, 1849 (1997)

6. R.K. Kirkwood, B.J. MacGowan, D.S. Montgomery, B.B. Afeyan, W.L. Kruer, D.M. Pennington, S.C. Wilks, J.D. Moody, K. Wharton, C.A. Back, K.G. Estabrook, S.H. Glenzer, M.A. Blain, R.L. Berger, D.E. Hinkel, B.F. Lasinski, E.A. Williams, D. Munro, B.H. Wilde, and C. Rousseaux, Phys. Plasmas **4**, 1800 (1997)

7. B.J. MacGowan, B.B. Afeyan, C.A. Back, R.L. Berger, G. Bonnaud, M. Casanova, B.I. Cohen, D.E. Desenne, D.F. Dubois, A.G. Dulieu, K.G. Estabrook, J.C. Fernández, S.H. Glenzer, D.E. Hinkel, T.B. Kaiser, D.H. Kalantar, R.L. Kauffman, R.K. Kirkwood, W.L. Kruer, A.B. Langdon, B.F. Lasinski, D.S. Montgomery, J.D. Moody, D.H. Munro, L.V. Powers, H.A. Rose, C. Rousseaux, R.E. Turner, B.H. Wilde, S.C. Wilks, and E.A. Williams, Phys. Plasmas **3**, 2029(1996).

8. D.S. Montgomery, B.B. Afeyan, B.J. MacGowan, C.A. Back, S.H. Glenzer, R.K. Kirkwood, J.D. Moody, G.F. Stone, R.L. Berger, K.G. Estabrook, W.L. Kruer, B.F. Lasinski, D.H. Munro, and E.A. Williams, "Persistent anti-correlation of stimulated Raman and Brillouin scattering levels in laser-produced plasmas," submitted to Phys. Rev. Lett.

9. S.C. Wilks, W.L. Kruer, J. Denavit, K. Estabrook, D.E. Hinkel, D. Kalantar, A.B. Langdon, B.J. MacGowan, D.S. Montgomery, and E.A. Williams, Phys. Rev. Lett. **74**, 5048 (1995).

10. B. I. Cohen, B.F. Lasinski, A.B. Langdon, and E.A. Williams, Phys. Plasmas **4**, 956 (1997).

11. E.A. Williams, Bull. Amer. Phys. Soc., mWepI1.01, November (1997).

12. W.L. Kruer, S.C. Wilks, B.B. Afeyan, and R.K. Kirkwood, Phys. Plasmas **3**, 382 (1996).

13. B.B. Afeyan, Bull. Amer. Phys. Soc., 7R.08, November (1995).

14. A.V. Maximov, W. Rozmus, V.T. Tikhonchuk, D.F. Dubois, H.A. Rose, A.M. Rubenchik, Phys. Plasmas **3**, 1689 (1996).

15. H.A. Rose, Phys. Plasmas **4**, 437 (1997).

16. B.B. Afeyan, A.E. Chou, and W.L. Kruer, "New Regimes of parametric instabilities in plasmas with flat-topped and depleted tail velocity distribution functions," submitted to Phys. Rev. Lett.

17. E.M. Campbell, J.T Hunt, E.S. Bliss, D.R. Speck, and R.P. Drake, Rev. Sci. Instrum. **57**, 2101 (1986).

18. Y. Kato and K. Mima, Appl. Phys. B **29**, 186 (1982).

19. G. Zimmerman and W. Kruer, Comments Plasma Phys. Controlled Fusion **2**, 85 (1975).

20. R.L. Berger, E.A. Williams, A. Simon, Phys. Fluids B **1**, 414 (1989).

21. J. Denavit and D.W. Phillion, Phys. Plasmas **1**, 1971 (1994).

Figure Captions

Figure 1 - Schematic of a) LLNL gasbag and heater beam geometry, b) LANL gas-hohlraum and heater beam geometry. Plots of n_e/n_{cr}, T_e (keV), and v (mm/ns) along the interaction beam central ray are shown at 0.7 ns for a gasbag (c) and a gas-hohlraum (d) with a 1 atm C_5H_{12} gas fill.

Figure 2 - Time-resolved backscattered SRS and SBS spectra from a LLNL gasbag (a, b) and a LANL gas-hohlraum (c, d) for targets with $n_e/n_{cr} \sim 0.11$, and $\nu_{ia}/\omega_{ia} > 0.1$.

Figure 3 - Time-resolved SRS and SBS spectra from an "unstretched" gas-hohlraum (a, b) and a "stretched" gas-hohlraum that was 250 μm longer (c, d), both containing 1 atm C_3H_8. The disruption in "normal" SRS, onset of "blast-wave" SRS, and peak SBS are coincident and occur at 0.8 ns in the unstretched target. All these features are coincident at 1.0 ns in the stretched target, and is consistent with LASNEX predictions for the delay in blast-wave propagation.

Figure 4 - a) Contour image of a calculation of the SRS spatial gain rate $\kappa(z, \lambda)$ at 0.5 ns from LASNEX profiles of the plasma conditions for a C_5H_{12} gasbag. The contour image is plotted versus z(mm) and λ_s (nm) for SRS. The "blast-wave" region is clearly evident as longer wavelengths (higher n_e/n_{cr}) beyond z=0.9 mm. Calculations of the time-resolved SRS gain are shown in b) by integrating $\kappa(z, \lambda)$ over the entire region; and in c) by integrating $\kappa(z, \lambda)$ over a limited region. The SRS gain spectra shown in (c) qualitatively reproduce the experimental spectra (see Fig. 2a).

Figure 5 - Plot of SBS peak reflectivity and SRS reflectivity at that time versus n_e/n_{cr} for C_3H_8/C_5H_{12} gases (open and closed circles) and CO_2/CF_4 gases (open and closed triangles). An estimate for $k_{epw}\lambda_{De}$ is also shown.

Figure 6 - Normalized SBS spectra from gasbag experiments with CO_2/CF_4 (weak IAW damping). The SBS spectra clearly show broadening as average n_e/n_{cr} increases.

Figure 7 - Plot of the instantaneous SBS reflectivity and the measured normalized spectral width $\Delta\omega/\omega_{ia}$ are shown for a CO_2 gasbag (a), and a CF_4/C_4H_{10} gas-hohlraum (b). The data clearly show that the peak SBS reflectivity occurs when $\Delta\omega/\omega_{ia}$ is smallest, and SBS is low when $\Delta\omega/\omega_{ia}$ is large.

Figure 8 - (a) Typical plot of $M(v/c_s)$ is shown for calculations using Eqs. 2 and 3 for 5 modes with λ = 100 - 200 μm. Results of SBS gain calculations versus M_{RMS} for several values of ν_{ia}/ω_{ia} are shown in (b). Calculated SBS spectral width $\Delta\omega/\omega_{ia}$ versus M_{RMS} is shown for several values of ν_{ia}/ω_{ia} (c).

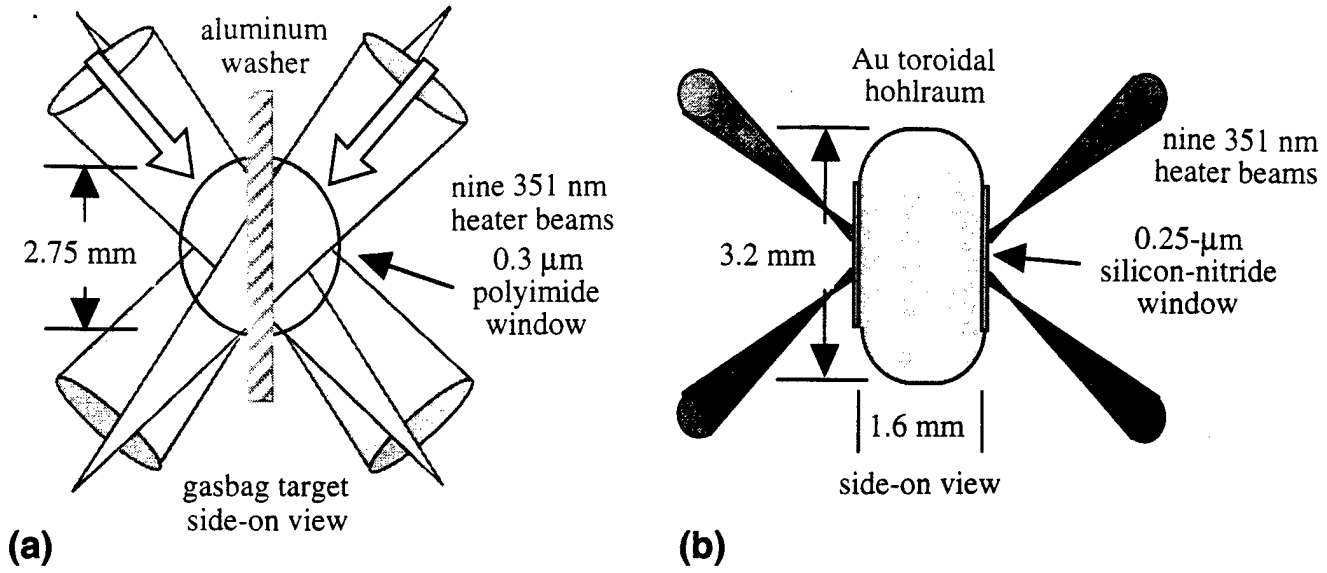
aluminum
washer
2.75 mm
nine 351 nm
heater beams
0.3 μm
polyimide
window
gasbag target
side-on view
(a)
Au toroidal
hohlraum
nine 351 nm
heater beams
3.2 mm
0.25-μm
silicon-nitride
window
1.6 mm
side-on view
(b)

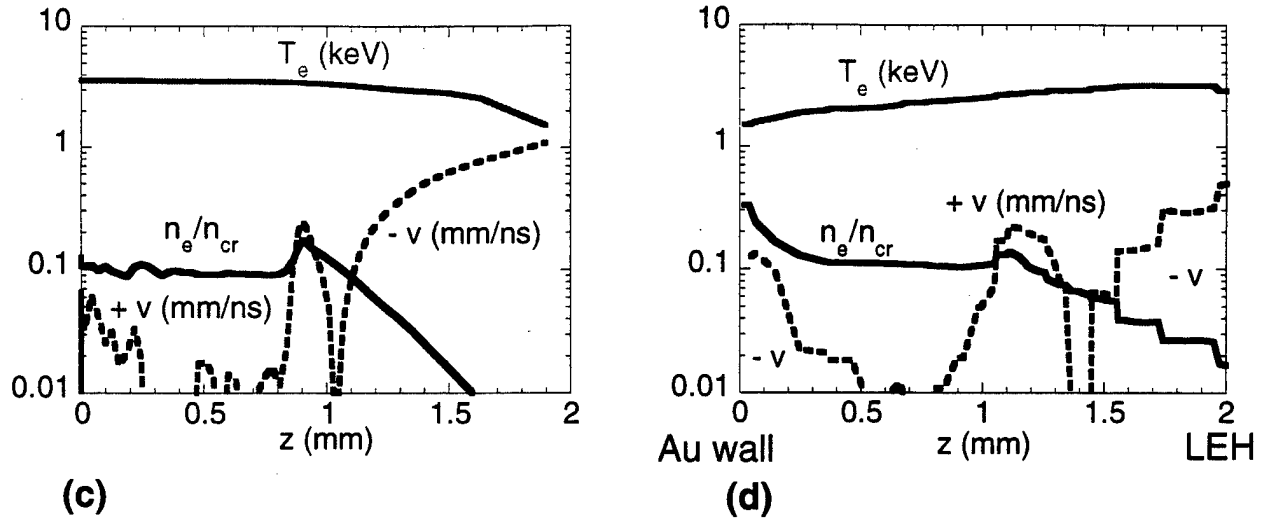
10
1
0.1
0.01
T_e (keV)
n_e/n_{cr}
- v (mm/ns)
+ v (mm/ns)
0
0.5
1
1.5
2
z (mm)
(c)
10
1
0.1
0.01
T_e (keV)
+ v (mm/ns)
n_e/n_{cr}
- v
- v
0
0.5
1
1.5
2
Au wall
z (mm)
LEH
(d)

Figures 1 a-d

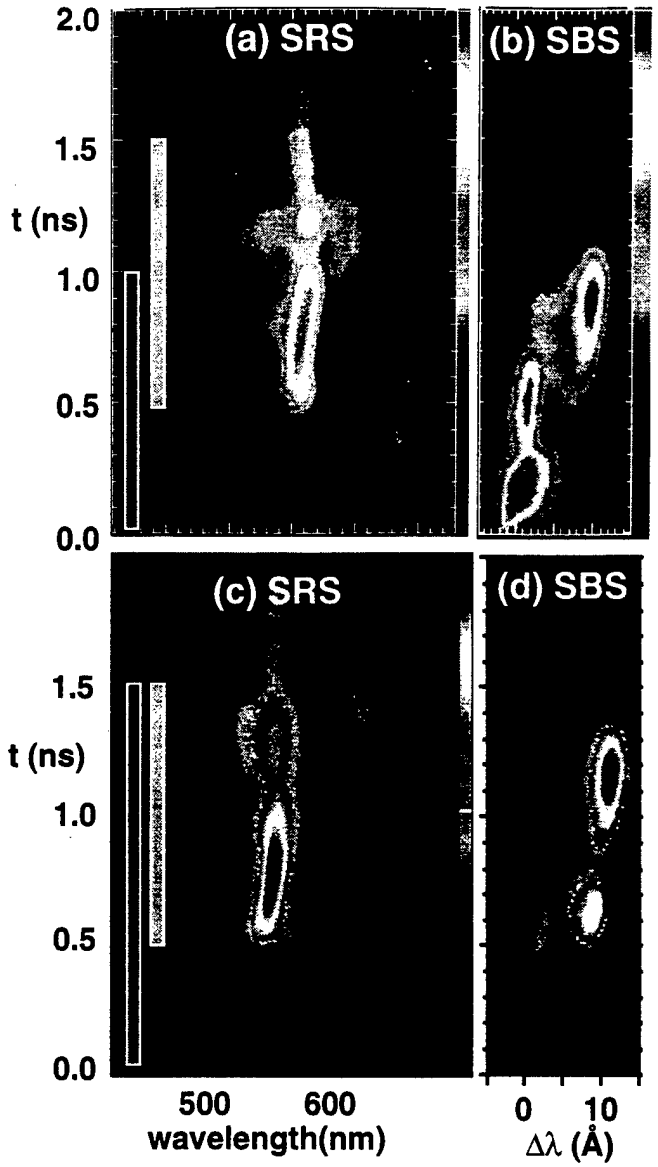
(a) SRS
(b) SBS
(c) SRS
(d) SBS
2.0
1.5
t (ns)
1.0
0.5
0.0
1.5
t (ns)
1.0
0.5
0.0
500
600
wavelength(nm)
0
10
Δλ (Å)

Figures 2 a-d

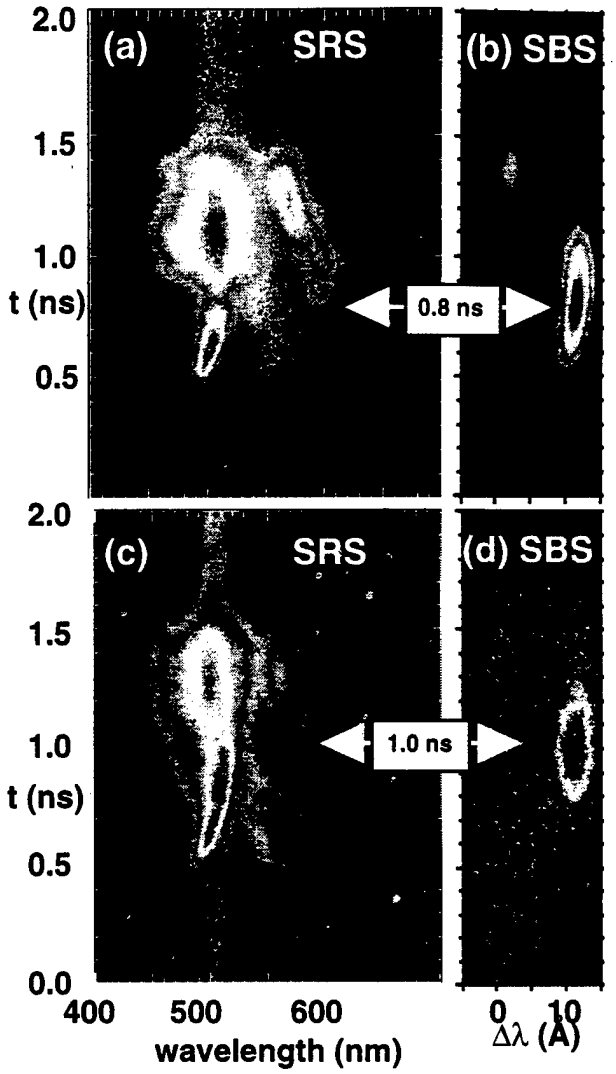
2.0
(a)
SRS
(b) SBS
1.5
1.0
t (ns)
0.8 ns
0.5
2.0
(c)
SRS
(d) SBS
1.5
1.0
1.0 ns
t (ns)
0.5
0.0
400
500
600
wavelength (nm)
0
10
Δλ (Å)

Figures 3 a-d

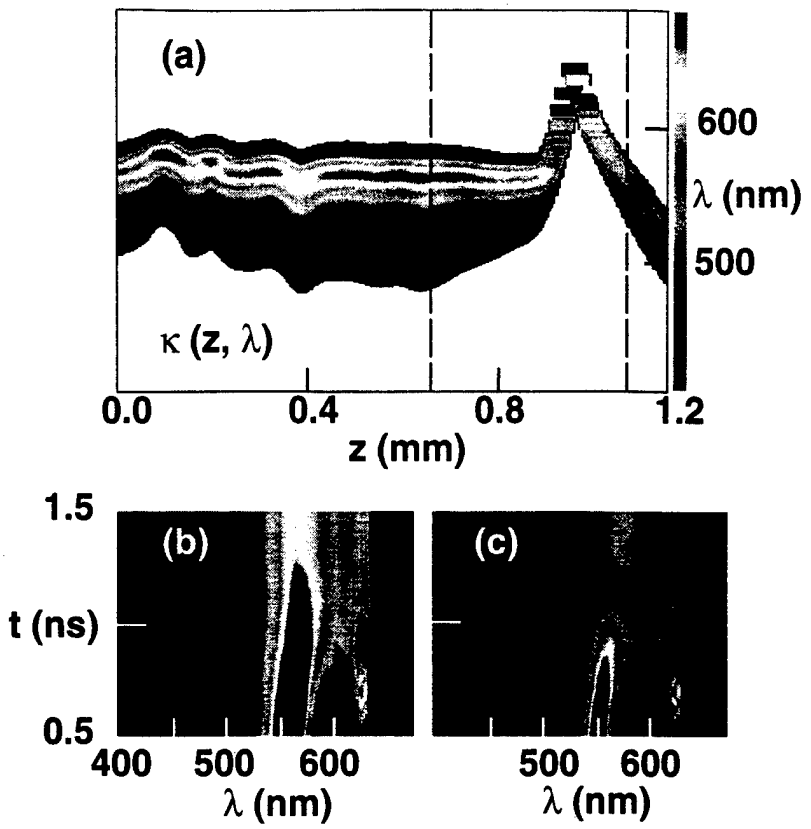
(a)
600
λ (nm)
500
κ (z, λ)
0.0
0.4
0.8
1.2
z (mm)
1.5
t (ns)
0.5
(b)
(c)
400
500
600
λ (nm)
500
600
λ (nm)

Figures 4 a - c

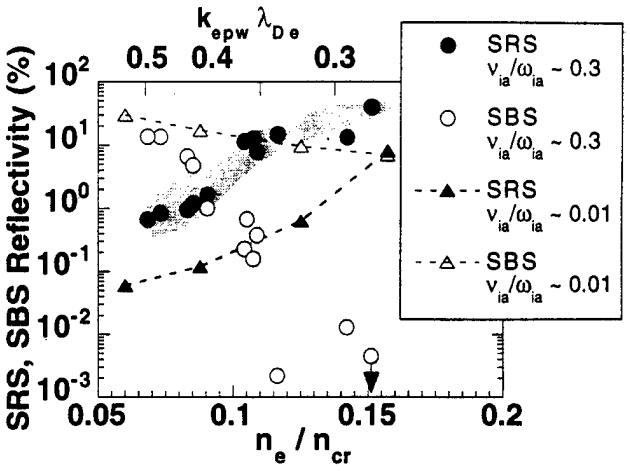
$k_{epw}\lambda_{De}$
0.5
0.4
0.3
SRS, SBS Reflectivity (%)
10^2
10^1
10^0
10^{-1}
10^{-2}
10^{-3}
0.05
0.1
0.15
0.2
n_e / n_{cr}
SRS ν_{ia}/ω_{ia} ~ 0.3
SBS ν_{ia}/ω_{ia} ~ 0.3
SRS ν_{ia}/ω_{ia} ~ 0.01
SBS ν_{ia}/ω_{ia} ~ 0.01

Figure 5

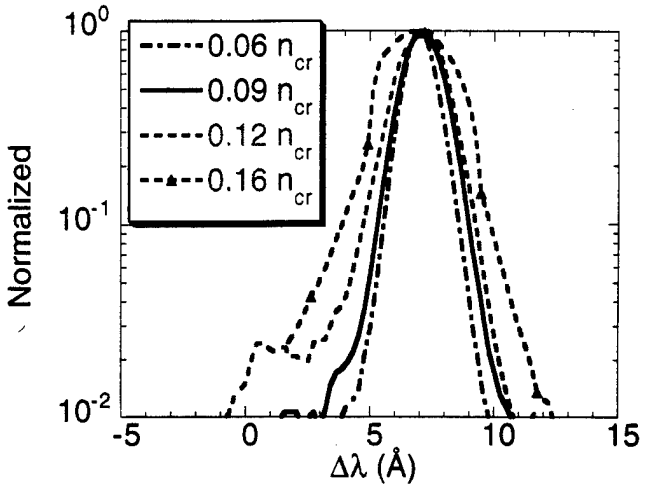
0.06 n_cr
0.09 n_cr
0.12 n_cr
0.16 n_cr
Normalized
10^0
10^-1
10^-2
-5
0
5
10
15
Δλ (Å)

Figure 6

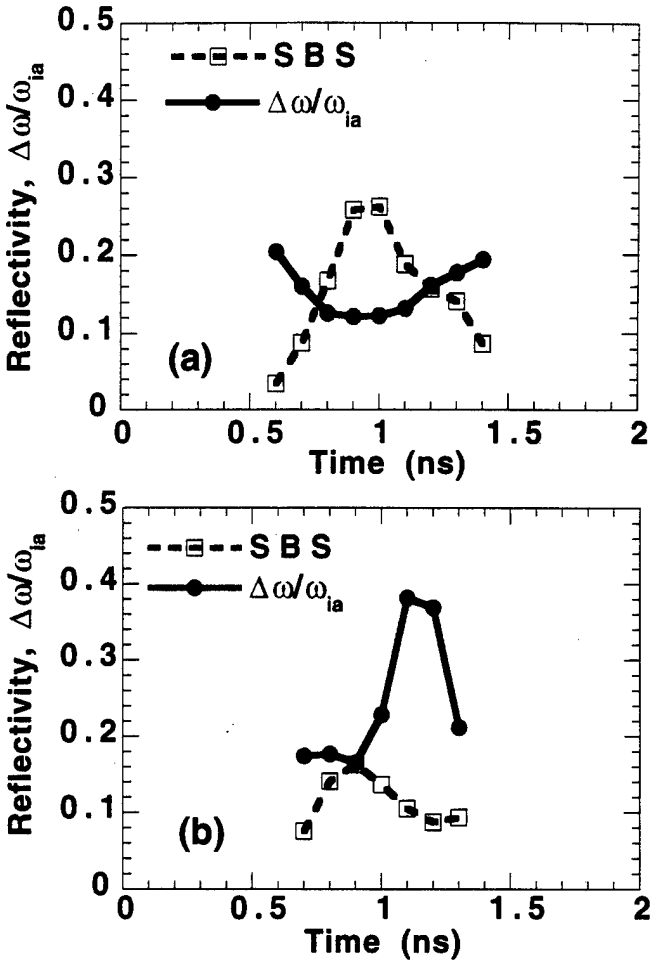
SBS
$\Delta\omega/\omega_{ia}$
Reflectivity, $\Delta\omega/\omega_{ia}$
(a)
(b)
Time (ns)
0
0.1
0.2
0.3
0.4
0.5
0.5
1
1.5
2

Figures 7 a-b

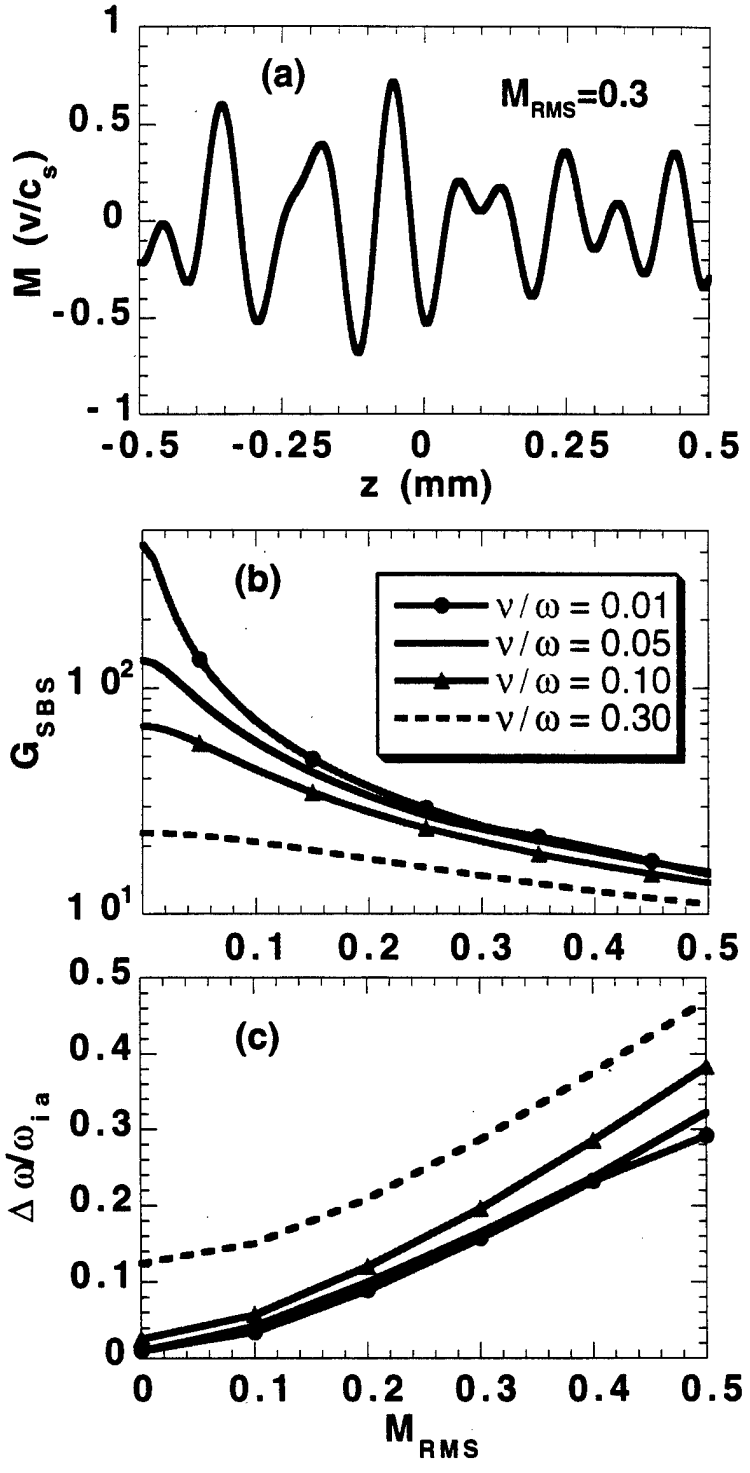
(a)
M_{RMS}=0.3
M (v/c_s)
z (mm)
(b)
ν/ω = 0.01
ν/ω = 0.05
ν/ω = 0.10
ν/ω = 0.30
G_{SBS}
(c)
Δω/ω_{ia}
M_{RMS}

Figures 8 a-c

Report Number (14) LA-UR-97-4830
CONF-971103--

Publ. Date (11) 199711
Sponsor Code (18) DOE/DP, XF
UC Category (19) UC-712, DOE/ER

DOE